COLLISION EFFICIENCY AND COLLOIDAL STABILITY OF UNEQUAL SIZE SPHERICAL PARTICLES MOVING THROUGH QUIESCENT VISCOUS LIQUID

SHINICHI YUU, FUYUHIKO NAKAGAWA, HIROSHI MIHARA AND YOSHIHIRO FUKUI

Laboratory of Powder Mechanics, Kyushu Institute of Technology, Kitakyushu 804

Key Words: Sedimentation, Solid Liquid Separation, Filtration, Colloidal Stability, Fluid Mechanics, Dust Collection

Collision efficiencies have been computed for unequal-size spherical particles settling in quiescent viscous liquids, taking into account the hydrodynamic interaction, interparticle attraction and electrostatic repulsion. The results are closely related to the mechanism of coagulation of colloidal particles in a sedimentation field. If the interparticle attraction and electrostatic repulsion are both negligibly small as compared to viscous drag, the collision efficiency η is very small, i.e. about 0.003. However, a relatively large Van der Waals force makes η greater than unity. As the ratio of the radii of the two particles (smaller divided by larger) decreases the collision efficiency also decreases. The repulsive force between particles determines whether the collision efficiency is zero or larger than zero, but it does not affect the magnitude of the collision efficiency. By including the effect of electrostatic repulsion we were able to develop criteria which determine the stability (or flocculation) of colloidal particles.

Introduction

The collision efficiency for unequal-size particles moving through viscous liquid is of importance for the estimation of coagulation rate of small particles settling in a water filtration pool, a lake or a marsh. It is valuable for study of the mechanisms of turbulent coagulation in a liquid flow.

For equal-size spherical particles in a shear flow, Curtis and Hocking[3] derived the collision efficiency and calculated the London–Hamaker constant from it. Lin *et al.*,[8] Batchelor and Green,[1] Van de Ven and Mason[11] and Zeichner and Schowalter[13] all calculated the trajectories of pairs of equal-size spherical particles in a shear flow. In addition, Zeichner and Schowalter's calculation includes particles in a uniaxial extensional flow. Van de Ven and Mason, and Zeichner and Schowalter showed the effect of hydrodynamic interaction, interparticle attraction and electrostatic repulsion. Zeichner and Schowalter determined the stability criteria for both shearing and extensional flows and showed that the results for these two flows are superposable by a suitable transformation of the flow strength axis. Higashitani *et al.*[6] made an approximate calculation of the collision efficiency for unequal-size particles in a simple shear flow by using the asymptotic trajectory equations for regions where particle pairs are either very close to each other or very far apart. Recently Davis[4] calculated the collision efficiency for unequal-size particles by using Batchelor's expression[2] for the relative velocity of two spheres. He did not consider the electrostatic repulsive force. He made a comparison between the effects of Van der Waals forces and Maxwell slip in promoting collision between aerosol particles. Wacholder and Sather[12] obtained formulae that represent the velocity distribution of unequal-size spherical particles moving under gravity through a quiescent flow field. They were interested only in determining the flow field and, therefore, they considered only the hydrodynamic interaction.

We have expanded this in the present project to a study of the trajectories of unequal-size particles where the factors of hydrodynamic interaction, interparticle attraction, and electrostatic repulsion forces are all taken into account. The principal objective of this study is to find the mechanism of the collision of unequal-size particles moving in a quiescent viscous liquid and to present the collision efficiencies as they are related to the coagulation process. In those cases where the effect of electrostatic repulsion becomes important, specific criteria for the stability of dispersions are presented.

1. Hydrodynamic Interaction and Particle Trajectory Equation

The following assumptions are made in the present calculation: first, that the fluid is incompressible and

Received January 29, 1987. Correspondence concerning this article should be addressed to S. Yuu.

Newtonian and that it is unbounded and at rest far from the particles; also that the inertial force of the fluid is negligibly small in comparison with the viscous force; and finally that the particle inertias are negligibly small in comparison with the viscous and pressure forces acting on them. Brownian motion of particles is neglected. **Figure 1** shows the coordinate geometry of our calculation.

Under conditions of negligible particle inertia the trajectory equations are given by equating the total forces and couples exerted on the particles to zero.

$$F_{i,j}+\frac{4}{3}\pi a_i^3(\rho_p-\rho_f)g+F_v+F_R=0 \tag{1}$$

Since there are no external couples acting on the particles, the hydrodynamic couple is

$$T_i=0 \tag{2}$$

Equations (1) and (2) and Fig. 1 show that the translational motion of the particles lies in the plane of r and g and that the component of their rotational velocities is only that about the direction normal to the plane of r and g.

Spielman[10] derived the following relations and goes on to give the series solutions for K_1, K_2, λ_1 and λ_2.

$$F_{1,r}=-K_1u_{1,r}+\lambda_1u_{2,r} \tag{3}$$

$$F_{2,r}=-K_2u_{2,r}+\lambda_2u_{1,r} \tag{4}$$

O'Neill and Majumdar[9] derived the following relations and present the numerical values of f_{11}, f_{12}, $\cdots$, g_{21} and g_{22}.

$$F_{1,\theta}=-6\pi\mu a_1\{f_{21}(R,\bar{r})u_{1,\theta}+f_{22}(R^{-1},R^{-1}\bar{r})u_{2,\theta}+a_1f_{11}(R,\bar{r})\omega_1-a_1f_{12}(R^{-1},R^{-1}\bar{r})\omega_2\} \tag{5}$$

$$F_{2,\theta}=-6\pi\mu a_2\{f_{22}(R,\bar{r})u_{1,\theta}+f_{21}(R^{-1},R^{-1}\bar{r})u_{2,\theta}+a_2f_{12}(R,\bar{r})\omega_1-a_2f_{11}(R^{-1},R^{-1}\bar{r})\omega_2\} \tag{6}$$

$$T_1=-8\pi\mu a_1^2\{g_{21}(R,\bar{r})u_{1,\theta}+g_{22}(R^{-1},R^{-1}\bar{r})u_{2,\theta}+a_1g_{11}(R,\bar{r})\omega_1-a_1g_{12}(R^{-1},R^{-1}\bar{r})\omega_2\} \tag{7}$$

$$T_2=-8\pi\mu a_2^2\{-g_{22}(R,\bar{r})u_{1,\theta}-g_{21}(R^{-1},R^{-1}\bar{r})u_{2,\theta}-a_2g_{12}(R,\bar{r})\omega_1+a_2g_{11}(R^{-1},R^{-1}\bar{r})\omega_2\} \tag{8}$$

The Van der Waals attractive force[5] between two particles is

$$F_v=-\frac{dE_v}{dr}=-\frac{1}{2a_1}\frac{dE_v}{dx}=-\frac{A}{24a_1}\left\{\frac{R(2x+R+1)}{(x^2+Rx+x)^2}+\frac{R(2x+R+1)}{(x^2+Rx+x+R)^2}-\frac{2R(2x+R+1)}{(x^2+Rx+x)(x^2+Rx+R+x)}\right\} \tag{9}$$

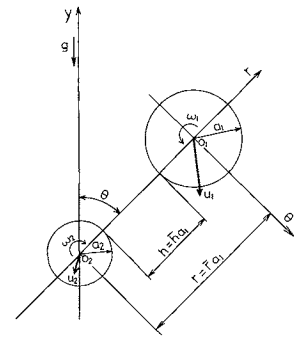

Fig. 1. Coordinates.

where $x=h/2a_1=\bar{h}/2$.

All the calculations reported here are those for an unretarded case.

The electrostatic repulsive force[7] is

$$F_R=-\frac{dE_R}{dr}=-\frac{dE_R}{a_1d\bar{h}}=4\pi\varepsilon\zeta^2\frac{R}{1+R}\frac{\bar{K}\exp(-\bar{K}\bar{h})}{1+\exp(-\bar{K}\bar{h})}. \tag{10}$$

Substituting Eqs. (3)–(10) into Eqs. (1) and (2), we obtain the following:

for particle 1,

$$\left.\begin{aligned}\left(\frac{d\bar{r}}{d\bar{t}}\right)_1&=-\bar{V}_{1,r}\cos\theta+\frac{1}{N_F\beta_1}(f_v+N_Rf_R)\\ \left(\bar{r}\frac{d\theta}{d\bar{t}}\right)_1&=\bar{V}_{1,\theta}\sin\theta\end{aligned}\right\} \tag{11}$$

for particle 2,

$$\left.\begin{aligned}\left(\frac{d\bar{r}}{d\bar{t}}\right)_2&=-\bar{V}_{2,r}\cos\theta-\frac{1}{N_F\beta_2}(f_v+N_Rf_R)\\ \left(\bar{r}\frac{d\theta}{d\bar{t}}\right)_2&=\bar{V}_{2,\theta}\sin\theta,\end{aligned}\right\} \tag{12}$$

where

$$\left.\begin{aligned}&\bar{r}=r/a_1,\ \bar{t}=u_{1,\infty}t/a_1,\ \bar{V}_{1,r}=6\pi\mu a_1\left(\frac{K_2+R^3\lambda_1}{K_1K_2-\lambda_1^2}\right),\\ &\bar{V}_{1,\theta}=\left(\frac{1}{L_{11}}+\frac{R^3}{L_{12}}\right),\quad \bar{V}_{2,r}=6\pi\mu a_1\left(\frac{\lambda_1+R^3K_1}{K_1K_2-\lambda_1^2}\right),\\ &V_{2,\theta}=\left(\frac{1}{L_{21}}+\frac{R^3}{L_{22}}\right),\quad \beta_1=\frac{K_1K_2-\lambda_1^2}{6\pi\mu a_1(K_2-\lambda_1)},\\ &\beta_2=\frac{K_1K_2-\lambda_1^2}{6\pi\mu a_1(K_1-\lambda_1)},\quad f_v=\frac{a_1}{A}F_v,\quad f_R=F_R/4\pi\varepsilon\zeta^2,\\ &N_F=6\pi\mu a_1^2u_{1,\infty}/A \text{ and } N_R=4\pi\varepsilon\zeta^2a_1/A.\end{aligned}\right\} \tag{13}$$

$$L_{11}=J/\Big\{Rf_{21}(R^{-1},R^{-1}\bar{r})[Rg_{11}(R,\bar{r})g_{22}(R^{-1},R^{-1}\bar{r})$$
$$-R^{-2}g_{12}^2(R^{-1},R^{-1}\bar{r})]$$
$$+\frac{3}{4}R^3f_{12}(R,\bar{r})[R^2f_{12}(R,\bar{r})g_{22}(R^{-1},R^{-1}\bar{r})$$
$$-R^{-1}f_{11}(R^{-1},R^{-1}\bar{r})g_{12}(R^{-1},R^{-1}\bar{r})]$$
$$+\frac{3}{4}R^3f_{11}(R^{-1},R^{-1}\bar{r})[f_{12}(R,\bar{r})$$
$$\times R^{-1}g_{12}(R^{-1},R^{-1}\bar{r})$$
$$-f_{11}(R^{-1},R^{-1}\bar{r})R^{-1}g_{11}(R,\bar{r})]\Big\}$$

$$L_{12}=L_{21}=J/\Big\{f_{22}(R^{-1},R^{-1}\bar{r})$$
$$\times[Rg_{11}(R,\bar{r})g_{22}(R^{-1},R^{-1}\bar{r})$$
$$-R^{-2}g_{12}^2(R^{-1},R^{-1}\bar{r})]$$
$$-\frac{3}{4}Rf_{11}(R,\bar{r})[R^2f_{12}(R,\bar{r})g_{22}(R^{-1},R^{-1}\bar{r})$$
$$-f_{11}(R^{-1},R^{-1}\bar{r})R^{-1}g_{12}(R^{-1},R^{-1}\bar{r})]$$
$$+R^2g_{22}(R,\bar{r})[f_{12}(R,\bar{r})$$
$$\times g_{12}(R^{-1},R^{-1}\bar{r})-f_{11}(R^{-1},R^{-1}\bar{r})g_{11}(R,\bar{r})]\Big\}$$

$$L_{22}=J/\Big\{-f_{21}(R,\bar{r})[Rg_{11}(R,\bar{r})g_{22}(R^{-1},R^{-1}\bar{r})$$
$$-R^{-2}g_{12}^2(R^{-1},R^{-1}\bar{r})]$$
$$+\frac{3}{4}f_{11}(R,\bar{r})[Rf_{11}(R,\bar{r})g_{22}(R^{-1},R^{-1}\bar{r})$$
$$-R^{-2}f_{12}(R^{-1},R^{-1}\bar{r})$$
$$\times g_{12}(R^{-1},R^{-1}\bar{r})]+\frac{3}{4}R^{-2}f_{12}(R^{-1},R^{-1}\bar{r})$$
$$\times[f_{11}(R,\bar{r})g_{12}(R^{-1},R^{-1}\bar{r})$$
$$-f_{12}(R^{-1},R^{-1}\bar{r})g_{11}(R,\bar{r})]\Big\}$$

in which

$$J=Q_1f_{21}(R^{-1},R^{-1}\bar{r})-2Q_2f_{22}(R^{-1},R^{-1}\bar{r})$$
$$-\frac{3}{4}R[f_{11}(R,\bar{r})f_{11}(R^{-1},R^{-1}\bar{r})$$
$$+f_{12}(R,\bar{r})g_{12}(R^{-1},R^{-1}\bar{r})]$$
$$-\frac{4}{3R^2}[Rf_{21}(R,\bar{r})f_{21}(R^{-1},R^{-1}\bar{r})$$
$$-f_{22}^2(R^{-1},R^{-1}\bar{r})][Rg_{11}(R,\bar{r})g_{22}(R^{-1},R^{-1}\bar{r})$$
$$-R^{-2}g_{12}^2(R^{-1},R^{-1}\bar{r})]$$

and

$$Q_1=f_{11}(R,\bar{r})g_{22}(R^{-1},R^{-1}\bar{r})$$
$$-2R^{-3}f_{11}(R,\bar{r})f_{12}(R^{-1},R^{-1}\bar{r})$$
$$\times g_{12}(R^{-1},R^{-1}\bar{r})$$
$$+R^{-3}f_{12}^2(R^{-1},R^{-1}\bar{r})g_{11}(R,\bar{r})$$
$$Q_2=Rf_{11}(R,\bar{r})f_{12}(R,\bar{r})g_{22}(R^{-1},R^{-1}\bar{r})$$
$$-[f_{11}(R,\bar{r})f_{11}(R^{-1},R^{-1}\bar{r})$$
$$+f_{12}(R,\bar{r})f_{12}(R^{-1},R^{-1}\bar{r})]R^{-2}g_{12}(R^{-1},R^{-1}\bar{r})$$
$$+R^{-2}f_{12}(R^{-1},R^{-1}\bar{r})f_{11}(R^{-1},R^{-1}\bar{r})g_{11}(R,\bar{r})$$
$$Q_3=R^2f_{12}^2(R,\bar{r})g_{22}(R^{-1},R^{-1}\bar{r})$$
$$-R^{-1}f_{12}(R,\bar{r})f_{11}(R^{-1},R^{-1}\bar{r})$$
$$\times g_{12}(R^{-1},R^{-1}\bar{r})$$
$$+R^{-1}f_{11}^2(R^{-1},R^{-1}\bar{r})g_{11}(R,\bar{r})$$

Therefore, the dimensionless relative trajectory equations of two particles with relative velocity are

$$\left.\begin{aligned}\frac{d\bar{r}}{d\bar{t}}&=\left(\frac{d\bar{r}}{d\bar{t}}\right)_1-\left(\frac{d\bar{r}}{d\bar{t}}\right)_2\\&=-\bar{V}_r\cos\theta+\frac{1}{N_F\beta}(f_v+N_Rf_R)\\\bar{r}\frac{d\theta}{d\bar{t}}&=\bar{r}\left(\frac{d\theta}{d\bar{t}}\right)_1-\bar{r}\left(\frac{d\theta}{d\bar{t}}\right)_2=\bar{V}\sin\theta\end{aligned}\right\}\qquad(14)$$

in which

$$\bar{V}_r=\bar{V}_{1,r}-\bar{V}_{2,r},\quad \bar{V}_\theta=\bar{V}_{1,\theta}-\bar{V}_{2,\theta}\text{ and }\beta=\frac{\beta_1\beta_2}{\beta_1+\beta_2}.\qquad(15)$$

The equations fitting the values of $\bar{V}_r$, $\bar{V}_\theta$ and β obtained by substituting Spielman's solutions for K_1, K_2, λ_1 and λ_2, and by substituting O'Neill and Majumdar's numerical values of $f_{11}, f_{12}, \cdots, g_{21}$ and g_{22} into Eqs. (13) and (15) are shown in **Appendix 1**.

2. Calculated Results

2.1 Velocity distribution

$\bar{V}_r\cos\theta$, $\bar{V}_\theta\sin\theta$ and β in Eq. (14) are $\bar{r}$, and θ components of the relative velocity, and the resistance correction coefficient of two approaching spherical particles respectively under the combined action of gravitational settling and hydrodynamic interaction. The solid and the dotted lines in **Fig. 2** show the series solution of $\bar{V}_r$ and approximate values. **Figure 3** shows the calculated results for the resistance correction coefficient, β. The truncated error of the series solutions is 10^{-3}. The differences between the approximate results (dotted lines) and the series solutions (solid lines) are very small. $\bar{V}_r$ for two approaching

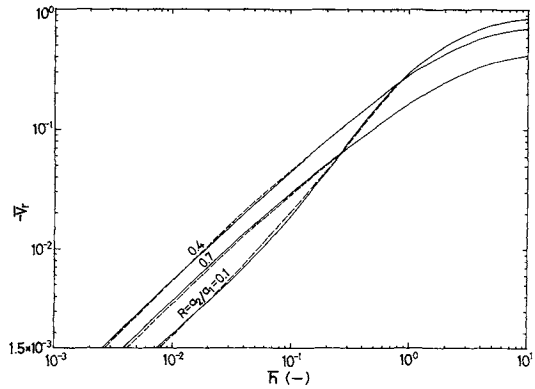

Fig. 2. Dimensionless function of radial component hydrodynamic relative velocity. ——, series solution; – – –, approximate values.

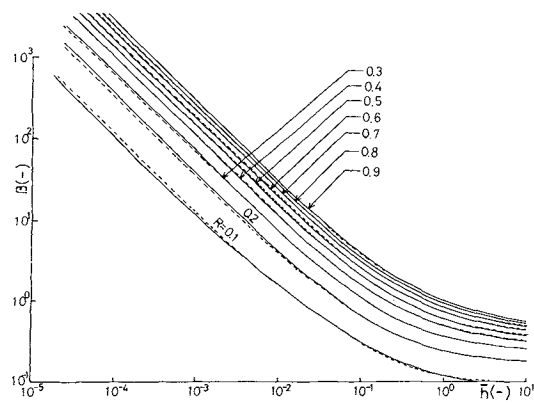

Fig. 3. Calculated resistance coefficient. ——, series solution; – – –, approximate values.

particles increases as the particle diameter ratio R decreases when their separation is large. However, at smaller separations the strong hydrodynamic interaction changes the trend as shown in Fig. 2. For example, the value of $\bar{V}_r$ for $R=0.7$ at $\bar{h} \leqq 10^{-1}$ is smaller than $\bar{V}_r$ for $R=0.4$. However, it becomes larger than $\bar{V}_r$ for $R=0.1$. When two particles are approaching, the presence of a larger particle increases the drag force on the smaller particle. The drag increase for a larger particle due to the existence of a smaller particle is much smaller. $\bar{V}_\theta$ decreases with increasing R for $\bar{h} \geqq 0.2$. However V_θ for $\bar{h}<2$ has a maximum at the region $0.3 \leqq R \leqq 0.5$. The results for $\bar{V}_\theta$ are omitted here due to limited space.

2.2 Particle trajectory and collision efficiency

Based on the initial conditions, i.e. $t=0$, $\bar{r}=\bar{r}_0$ and $\theta=\theta_0$, numerical integration of Eq. (14) using an algorithm of Runge-Kutta-Merson gives the relative trajectories of two spherical particles as they fall in a quiescent fluid. **Figure 4** shows some examples of relative trajectories for $N_F=10^5$, $N_R=0$, and $R=0.5$. It can be seen that the larger particle moves downward relative to the smaller one, either colliding or passing around and below it.

The trajectory equation Eq. (14) was solved, start-

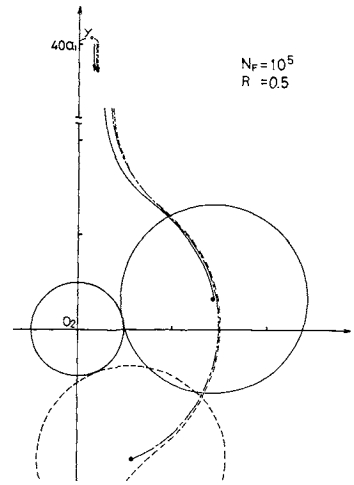

Fig. 4. Particle relative trajectory.

ing with a large initial value of $\bar{r}_0$ and with different initial values of $\bar{y}_0$. The minimum distance $\bar{r}$ between the centers of the particles can be found for each trajectory. By varying $\bar{y}_0$, a critical value $\bar{y}_c$ was found for which the minimum gap $\bar{r}-1-R$ was equal to zero. The collision efficiency η is then given by

$$\eta=(\bar{y}_c/(1+R))^2 . \tag{16}$$

When making the trajectory calculation to determine the collision efficiency, one should choose the initial value of $\bar{r}_0$ so large that the effect of hydrodynamic and interparticle forces essentially vanish. **Figure 5** shows the effect of $\bar{r}_0$ on η. The calculated result indicates that the effect on η is very small when $\bar{r}_0$ is larger than 40. Hence, we chose this as the initial value of $\bar{r}_0$ and allowed it to decrease from there.

Figure 6 shows the calculated results of collision efficiency η for $N_R=0$. For smooth particles with clean surfaces, the minimum separation distance δ_m is typically 0.4 nm. Thus if $a_1=1\,\mu$m, $\bar{\delta}_m=0.4\,\text{nm}/1\,\mu\text{m}=4\times10^{-4}$. As mentioned later from calculated results, the critical separation distance δ_c at which collisions are bound to occur due to the attractive force is actually much larger than 0.4 nm by Van der Waals attractive force. N_F describes generally the relation of the hydrodynamic forces to the attractive force. For example, N_F is defined as

$$N_F=\frac{4}{3}\pi a_1^4(\rho_p-\rho_f)g/A$$

for gravitational settlig, and

$$N_F=\frac{4}{3}\pi a_1^4(\rho_p-\rho_f)r\omega^2/A$$

for centrifugal settling. A small value of N_F indicates a relative large Van der Waals attractive force compared to the hydrodynamic force. As shown in Fig. 6, a relatively large Van der Waals force with $N_F=0.1$

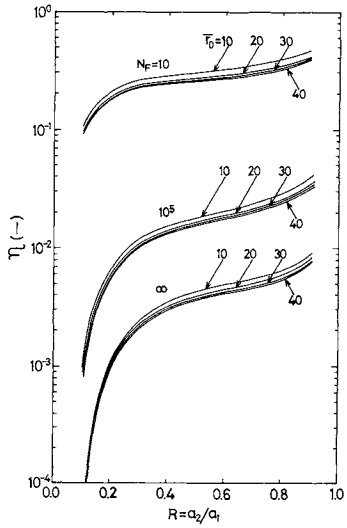

Fig. 5. Calculated results of collision efficiency ($\delta = 4 \times 10^{-4}$ for $N_F = \infty$).

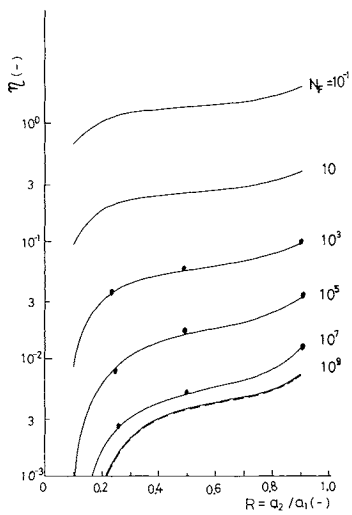

Fig. 6. Calculated results of collision efficiency. ----, $N_F = \infty$; ●, calculated results by Davis.[4]

makes η greater than unity. At this value of N_F, a_1 is equal to 0.7 μm for gravitational settling when the density difference between particle and fluid is 0.1 g/cm^3 and A is 10^{-20} joule. On the other hand, when $N_F = 10^9$, which means $a_1 = 220\,\mu$m for gravitational settling, the curve is essentially identical with $N_F =$ infinity. Under these conditions the effect of the Van der Waals force on η is negligibly small.

The value of η depends upon the particle size ratio $R = a_2/a_1$, that is, η increases as R increases to unity. This is because the hydrodynamic resistance forces for two approaching particles decreases and the Van der Waals attractive force described in Eq. (9) increases. The rate of change of the Van der Waals attractive force with a change in R is smaller than that of the hydrodynamic interaction force. This means that the change of η with R for small N_F, where the Van der Waals force is the dominant mechanism of particle collisions, is much smaller than that occurring with a large N_F. Points marked ● in Fig. 6 are calculated results by Davis.[4] Our results are in good agreement with Davis.

Figure 7 shows the effect of $\bar{\delta}$ on η at various values of N_F. The result indicates that as the Van der Waals attractive force increases, thereby decreasing N_F, δ_c increases rapidly. δ_c for zero attractive force is equal to $\delta_m = 0.4$ nm, so that δ_c is usually much larger than the minimum separation δ_m. For example, $\bar{\delta}_c$ for $N_F = 10^5$, which means a fairly small Van der Waals attractive force, is 8×10^{-3} as shown in Fig. 7. When a_1 is 10 μm, $\delta_c = a_1 \bar{\delta}_c$ is 80 nm.

Our calculated results for η are compared with those (marked × in **Fig. 8**) obtained by Zeichner and Schowalter[13] for simple shear flow in Fig. 8. They calculated η for two equal-size spherical particles. Our calculations are for two unequal spheres moving under gravity through quiescent viscous flow, so η for equal-size particles ($R = 1$) does not exist in our calculation. In their calculation Zeichner and Schowalter used $\bar{r}_o = 10$, and our results in Fig. 8 were therefore calculated under the same initial condition and extrapolated to give Zeichner and Schowalter's values for η shown by the points in the figure marked ×, which represent the place where $R = 1$.

2.3 Stability of colloidal particles

We used our method to determine the conditions under which a suspension is completely stable for a given flow strength. This means that the collision efficiency is zero and that collisions do not occur for a pair of unequal-size particles whose centers are aligned with each other in the direction of gravity. By calculating the critical trajectory, which has the initial conditions $\bar{r} = \infty$ and $\theta = 0$, we were able to determine the strength of the repulsive force, as measured by N_R, necessary to prohibit coagulation at various flow strengths N_F. We started by considering a pair of unequal-size particles whose centerlines are aligned with the direction of gravity. A large particle approaches a small one until repulsion stops it at the point where the potential energy function is at a minimum. After that the large particle rotates around the small one until the large particle is directly below the smaller one (i.e. $\theta = 180°$) at which location the repulsion force is at a maximum because the gravity force is now added to the interparticle repulsive force. If the particles do not then separate, coagulation occurs at a distance at which the separation between particle surfaces is larger than the minimum separation of 0.4 nm. The doublet then forms a weakly bound aggregate. When the interparticle attractive force is larger or the repulsive force is smaller than in the above case, the large particle collides with the small one at the minimum separation, i.e. $\delta_m = 0.4$ nm, and rotates until $\theta = 180°$. If the pair of particles does

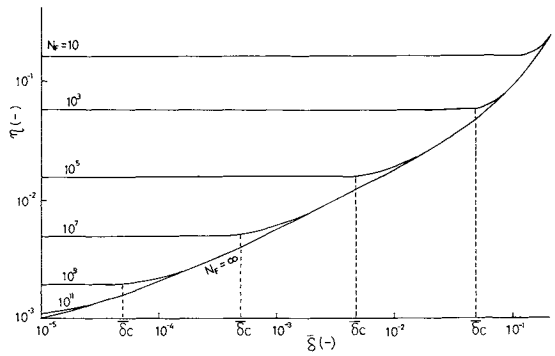

Fig. 7. η vs. δ.

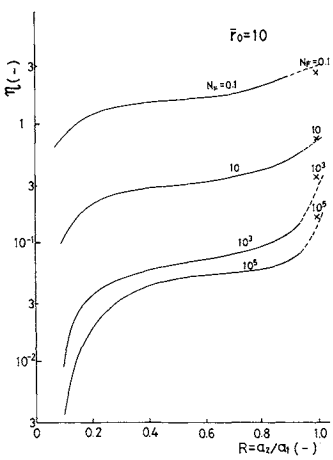

Fig. 8. η vs. R.

not separate there, coagulation occurs at the minimum separation and the doublet forms a strongly bound aggregate.

The critical condition for the strongly bounded coagulation is obtained by substituting $\bar{r}=1+R+\bar{\delta}_m$, $\theta=180°$ and $d\bar{r}/d\bar{t}=0$ into Eq. (14). If the minimum separation distance δ_m and the diameter of larger particle a_1 are 0.4 nm and 10 μm respectively, $\bar{\delta}_m$ is 4×10^{-5}. Further substitution of $\theta=180°$, $\bar{K}=10^4$ and $d\bar{r}/d\bar{t}=0$ into Eq. (14) gives

$$N_F=-(f_v+N_R f_R)/(\bar{V}_r\beta) \tag{17}$$

$$\begin{aligned} N_R&=2.60\times10^4-7.75\times10^{-6}N_F \quad \text{for} \quad R=0.1\\ N_R&=2.60\times10^4-5.07\times10^{-5}N_F \quad \text{for} \quad R=0.5\\ N_R&=2.60\times10^4-1.61\times10^{-5}N_F \quad \text{for} \quad R=0.9 \end{aligned} \tag{18}$$

When $d\bar{r}/d\bar{t}$ does not vanish at some separation that is larger than the minimum separation δ_m and when N_R is smaller than the value of Eq. (18), the colloidal particles form strongly bounded aggregates.

The results of numerical integration of the trajectory equations are presented as a stability plane N_R-N_F, with the ratio of particle radii R as a parameter. In all cases the stability plane was divided into five regions, as shown in **Fig. 9**. In region I_a, where strongly bound aggregation with minimum separation is expected, the effect of the repulsive force

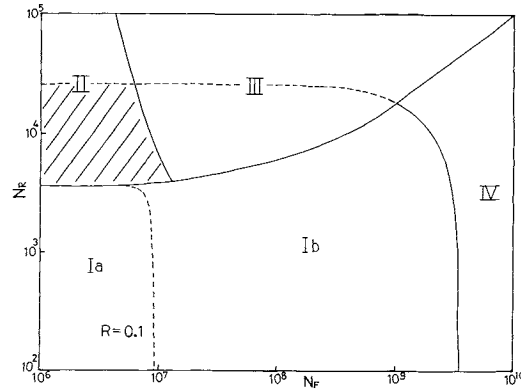

Fig. 9. Stability plane for $R=0.1$. $\bar{K}=10^4$ and $\bar{\delta}_m=4\times10^{-5}$.

on the collision efficiency is negligibly small. On the other hand, in region I_b where strongly bound aggregation with minimum separation is also expected, there is a slight dependency of the repulsive potential energy on the collision efficiency. In region II weakly bound aggregation occurs. In region III, $d\bar{r}/d\bar{t}$ for $\theta=0$ vanishes at the minimum in the potential energy function. However, the larger particle still rotates around the smaller one and separates. Therefore, the suspension is also stable in this region. In region IV, when a pair of unequal-size particles whose centerlines aligned with the direction of gravity ($\theta=0$) approach each other, they collide at the minimum separation distance. However, the larger particle in the pair rotates around the smaller one and then separates. Therefore there should be no flocculation and the suspension is stable to flow in this region.

Considering centrifugal force as a variable external force which causes a relative velocity between unequal-size particles, N_F increases with increasing rotation speed. On the other hand, N_R remains constant since it is independent of external force, as seen in Eq. (13). For interpretation of the results in the stability plane, consider a situation in which doublets are present in a suspension for $N_R=10^4$ as in Fig. 9. If the rotation speed is gradually increased the aggregate will first deflocculate out of the weakly bound state and then reflocculate into strongly bound aggregates. At a higher rotation speed aggregates will deflocculate from then minimum separation distance.

Consider another situation in which N_R is gradually decreased by adding a coagulant under conditions where K and δ_m are constant. If we set $N_F=5\times10^6$ and if N_R is decreased from its value of 10^5 in Fig. 9, colloidal particles will first flocculate into weakly bound aggregate and then reflocculate into strongly bound aggregate.

Experiments should be done to verify the calculated results of stability criteria, since there are no experimental data available for comparison.

When interparticle energy curve (E_v+E_R) is a

linearly increasing function, the resultant interparticle force is attractive at any separation distance, and the colloidal particles then form strongly bound aggregates. This case corresponds to interparticle potential energy in regions I_a and I_b. When the potential energy function has a minimum value whose distance from the particle surface is greater than the minimum distance δ_m (i.e. 0.4 nm), colloidal particles form weakly bound aggregates. This case corresponds to the interparticle potential energy in region II at the configuration where the larger particle is below the smaller one. The potential energy function in the shaded area in Fig. 9 has both a primary and a secondary minimum. In this region colloidal particles usually form weakly bound aggregates at the secondary minimum. If the interparticle potential energy curve is continually decreasing, the resultant interparticle force is repulsive for any separation distance and the suspension is then stable. This case corresponds to the interparticle potential energies in regions III and IV of Fig. 9 in the configuration where the larger particle is directly below the smaller one.

Figure 10 shows the effect of repulsive potential energy on the collision efficiency in region I_b. The results indicate that in this region there is only a minor dependency on the collision efficiency. Since the repulsive potential energy between particles is short-range, it determines whether the collision efficiency is zero or larger than zero, but it does not affect the magnitude of the collision efficiency.

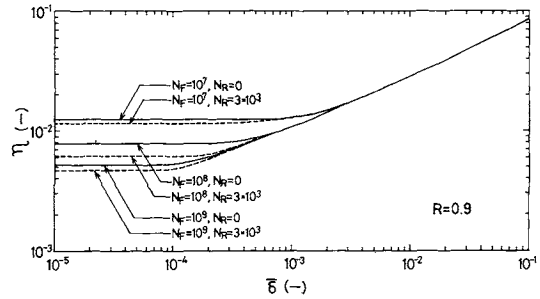

Fig. 10. Effect of repulsive potential energy on collision efficiencies in Region I_b. $\bar{K}=10^4$.

Appendix 1

The fitting equations of $\bar{V}_r$, $\bar{V}_\theta$, and β used in the particle trajectory calculation are

$$\bar{V}_r=1-R^2+\frac{3}{2}\frac{(R^3-1+q_1)}{\bar{r}}-\frac{1}{2}\frac{(R^2+1)(R^3-1)+q_2}{\bar{r}^3}+\frac{q_3}{\bar{r}^6}$$

for $h\geqq 0.2$ (A1)

where

$$q_1=-0.00677\,R^{-1.01}$$

$$q_2=0.493R^3-0.743R^2+0.225R-0.0414$$

$$q_3=4.83R^3-6.94R^2+1.32R+0.0146\,,$$

$$\bar{V}_r=(0.434R^3-1.35R^2+0.660R+0.248)\bar{h}^{\{-2.18(R-0.780)^5+0.837\}}$$

for $0.04\leqq\bar{h}\leqq 0.2$ (A2)

$$\bar{V}_r=(1.78R^3-4.61R^2+2.95R-0.102)\bar{h}^{(0.08\,R^{0.3}+0.9)}$$

for $h\leqq 0.04$ (A3)

$$\bar{V}_\theta=1-R^2+\frac{3}{4}\frac{(R^3-1)}{\bar{r}}+\frac{1}{4}\frac{(R^3-1)(R^2+1)}{\bar{r}^3}+\frac{(2R^2-1.86R+0.2)}{\bar{r}^6}$$

for $\bar{h}\geqq 0.02$ (A4)

$$\bar{V}_\theta=\frac{\bar{V}_{\theta|\bar{h}=0.02}-\bar{V}_{(T)}}{0.02^{(0.375R^2-0.478R+0.208)}}\bar{h}^{(0.375R^2-0.478R+0.208)}+\bar{V}_{(T)}$$

for $\bar{h}\leqq 0.02$ (A5)

where $\bar{V}_{(T)}$ calculated by Wacholder and Sather[12] is the tangential velocity due to the rigid body rotation of two touching spheres. The fitting equation of $\bar{V}_{(T)}$ is

$$\bar{V}_{(T)}=-0.456R^3+0.257R^2+0.206R-0.0096\,. \quad \text{(A6)}$$

The fitting equations of β are

$$\begin{aligned}
&\beta=0.0123\bar{h}^{-0.97} && \text{for } R=0.1 \text{ and } \bar{h}\leqq 10^{-2}\\
&\beta=0.172\bar{h}^{-0.97} && \text{for } R=0.5 \text{ and } \bar{h}\leqq 10^{-2}\\
&\beta=0.330\bar{h}^{-0.97} && \text{for } R=0.9 \text{ and } \bar{h}\leqq 10^{-2}
\end{aligned} \quad \text{(A7)}$$

Other equations for β used in the calculation are omitted to save space. The fitting errors are within 1%.

Nomenclature

A	=	Hamaker constant	[J]
a_1, a_2	=	radii of larger and smaller particles	[μm]
a_i	=	radius of particle i	[μm]
E_R, E_v	=	repulsive and attractive potential energies	[J]
$F_{i,j}$	=	j component of hydrodynamic force exerted on particle i	[N]
F_R, F_v	=	interparticle repulsive and attractive forces	[N]
f_{ij}, g_{ij}	=	resistance coefficients presented by O'Neill and Majumdar[9]	[—]
f_R, f_v	=	dimensionless interparticle repulsive and attractive forces defined by Eq. (13)	[—]
g	=	gravitational acceleration	[m/s^2]
h	=	$r-(a_1+a_2)$, separation between particle surfaces	[μm]
$\bar{h}$	=	h/a_1	[—]
$J, L_{ij}Q_i$	=	resistance coefficient functions	[—]
$\bar{K}$	=	$a_1\kappa$, double-layer thickness parameter	[—]
$K_1, K_2, \lambda_1, \lambda_2$	=	Spielman's resistance coefficient[10]	[—]
N_F	=	$6\pi\mu a_1^2 u_{1,\infty}/A$, dimensionless parameter describing the relative importance of hydrodynamic force to attractive force	[—]
N_R	=	$4\pi\varepsilon\zeta^2 a_1/A$, dimensionless parameter describing the relative importance of repulsive forces to attractive force	[—]
R	=	a_2/a_1, ratio of smaller to larger particle radii	[—]
$r, \bar{r}$	=	separation distance between particle centers, radial coordinate and its dimensionless form	[m], [—]
$\bar{r}_0$	=	dimensionless initial value of r for trajectory calculation	[m]
T_i	=	hydrodynamic couple about O_i shown in Fig. 1	[N]
$t, \bar{t}$	=	time and its dimensionless form	[s], [—]
$u_{1,\infty}$	=	$2(\rho_p-\rho_f)ga_1^2/9\mu$, Stokes settling velocity of larger particle	[m/s]
$u_{i,r}, u_{i,\theta}$	=	radial and tangential velocity components	

of particle i [m/s]

$\bar{V}_{ij}$ = dimensionless function of j component hydrodynamic velocity of particle i [—]

$\bar{V}_j$ = dimensionless function of j component hydrodynamic relative velocity [—]

$\bar{V}_T$ = dimensionless function of tangential velocity due to the rigid-body rotation of two touching spheres [—]

$\bar{y}_0, \bar{y}_c$ = dimensionless initial value for trajectory calculation [—]

β = $\beta_1\beta_2/(\beta_1+\beta_2)$, resistance coefficient [—]

β_1, β_2 = resistance coefficients defined by Eq. (13) [—]

$\delta, \bar{\delta}$ = particle surface separation distance under which we suppose that collisions occur and its dimensionless form

$\delta_c, \bar{\delta}_c$ = maximum particle surface separation distance under which collisions are bound to occur and its dimensionless form

$\delta_m, \bar{\delta}_m$ = minimum separation distance $\fallingdotseq$ 0.4 nm and its dimensionless form

ε = dielectric constant [$J^{-1}m^{-1}$]

θ = angular spherical coordinate [—]

η = collision efficiency defined by Eq. (16) [—]

κ = reciprocal Debye length [m^{-1}]

μ = viscosity [kg/m·s]

ζ = ζ-potential [J]

ρ_f, ρ_p = fluid and particle densities [kg/m^3]

ω_i = angular velocity of particle i [s^{-1}]

ω = angular velocity of particle 1 due to external centrifugal force [s^{-1}]

Literature Cited

1) Batchelor, G. K. and J. T. Green: *J. Fluid Mech.*, **56**, 375 (1972).
2) Batchelor, G. K.: *J. Fluid Mech.*, **119**, 379 (1982).
3) Curtis, A. S. G. and L. M. Hocking: *Trans. Faraday Soc.*, **66**, 1381 (1970).
4) Davis, R. H.: *J. Fluid Mech.*, **145**, 179 (1984).
5) Hamaker, J. C.: *Physica*, **4**, 1058 (1937).
6) Higashitani K., R. Ogawa, G. Hosokawa and Y. Matsuno: *J. Chem. Eng. Japan*, **15**, 299 (1982).
7) Hogg, R., T. W. Healy and D. W. Fuerstenau: *Trans. Faraday Soc.*, **62**, 1638 (1966).
8) Lin, C. J., K. J. Lee and N. F. Sather: *J. Fluid Mech.*, **43**, 35 (1970).
9) O'Neill, M. E. and S. R. Majumdar: *ZAMP*, **21**, 164 (1970).
10) Spielman, L.A.: *J. Colloid Interface Sci.*, **45**, 55 (1973).
11) Van der Ven, T. G. M. and S. G. Mason: *J. Colloid Interface Sci.*, **57**, 505 (1976).
12) Wacholder, E. and N. F. Sather: *J. Fluid Mech.*, **65**, 417 (1974).
13) Zeichner, G. R. and W. R. Schowalter: *AIChE J.*, **23**, 243 (1977).

NUMERICAL ANALYSIS OF TERNARY MASS TRANSFER IN A LAMINAR BOUNDARY LAYER

HITOSHI KOSUGE, TSUTOMU ISHIKAWA AND KOICHI ASANO

Department of Chemical Engineering, Tokyo Institute of Technology, Tokyo 152

Key Words: Mass Transfer, Numerical Analysis, Laminar Boundary Layer, Ternary System, Diffusional Interaction, Reverse Diffusion

Numerical approaches to ternary mass transfer in a laminar boundary layer were made by use of a laminar boundary layer theory considering the effects of interactions between diffusion fluxes and of mass injection or suction.

The effects of both the driving force ratios and the multicomponent Schmidt numbers on the concentration profiles and the diffusion fluxes are discussed. A new correlation is proposed for the effect of the interactions between the diffusion fluxes under the condition of low mass flux and of zero tangential surface velocity, which is a function of the driving force ratios and the multicomponent Schmidt numbers. The possibility of a reverse diffusion was also shown under the same condition. Some examples of numerical analysis are presented for the effect of mass injection or suction and of the tangential surface velocity on the diffusion fluxes.

Introduction

The phenomenon of multicomponent mass transfer under flow conditions is a very complicated one, in which mass flux at the interface has some effect on the velocity, temperature and concentration profiles near the interface and interactions between diffusion fluxes of different species take place. Although some theoretical and experimental approaches[2,3,10-12,14-17] to multicomponent mass transfer under stationary conditions have been made, few approaches under the flow conditions have been reported.

Received February 7, 1987. Correspondence concerning this article should be addressed to H. Kosuge.